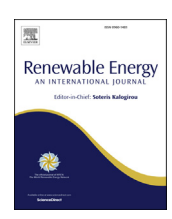
Contents lists available at ScienceDirect

Renewable Energy

journal homepage: www.elsevier.com/locate/renene



Heat depletion in sedimentary basins and its effect on the design and electric power output of CO₂ Plume Geothermal (CPG) systems



Benjamin M. Adams ^{a, b, *}, Daniel Vogler ^a, Thomas H. Kuehn ^b, Jeffrey M. Bielicki ^{c, d}, Nagasree Garapati ^{a, e}, Martin O. Saar ^{a, f, **}

- ^a Geothermal Energy and Geofluids Group, Department of Earth Sciences, ETH Zurich, Sonneggstrasse 5, 8092, Zürich, Switzerland
- b Department of Mechanical Engineering, University of Minnesota, 111 Church St SE, Minneapolis, MN, 55455, USA
- ^c Department of Civil, Environmental, and Geodetic Engineering, The Ohio State University, 2070 Neil Ave, Columbus, OH, 43210, USA
- ^d John Glenn College of Public Affairs, The Ohio State University, 1810 College Road, Columbus, OH, 43210, USA
- ^e Department of Chemical and Biomedical Engineering, West Virginia University, P.O. Box 6102, Morgantown, WV, 26506, USA
- Department of Earth and Environmental Sciences, University of Minnesota, 116 Church St SE, Minneapolis, MN, 55455, USA

ARTICLE INFO

Article history: Received 10 July 2020 Received in revised form 22 November 2020 Accepted 25 November 2020 Available online 2 December 2020

Keywords: CO₂ geothermal Geothermal electricity Reservoir heat depletion Sedimentary basin geothermal

ABSTRACT

CO₂ Plume Geothermal (CPG) energy systems circulate geologically stored CO₂ to extract geothermal heat from naturally permeable sedimentary basins. CPG systems can generate more electricity than brine systems in geologic reservoirs with moderate temperature and permeability. Here, we numerically simulate the temperature depletion of a sedimentary basin and find the corresponding CPG electricity generation variation over time. We find that for a given reservoir depth, temperature, thickness, permeability, and well configuration, an optimal well spacing provides the largest average electric generation over the reservoir lifetime. If wells are spaced closer than optimal, higher peak electricity is generated, but the reservoir heat depletes more quickly. If wells are spaced greater than optimal, reservoirs maintain heat longer but have higher resistance to flow and thus lower peak electricity is generated. Additionally, spacing the wells 10% greater than optimal affects electricity generation less than spacing wells 10% closer than optimal. Our simulations also show that for a 300 m thick reservoir, a 707 m well spacing provides consistent electricity over 50 years, whereas a 300 m well spacing yields large heat and electricity reductions over time. Finally, increasing injection or production well pipe diameters does not necessarily increase average electric generation.

© 2020 The Author(s). Published by Elsevier Ltd. This is an open access article under the CC BY license (http://creativecommons.org/licenses/by/4.0/).

1. Introduction

Global carbon dioxide (CO₂) emissions must be reduced by at least 78%-118% (when compared to 2010 emission levels) by 2100 in order to keep Earth's mean annual surface temperature increase within 2 °C of pre-industrial levels and thus avoid substantial negative environmental and economic consequences [1]. Several strategies have been identified to meet the CO₂ emissions reduction goal, and most include CO₂ capture and geologic storage (CCS) [2,3]. Additionally, CO₂ from electricity generation accounted for 40% of

E-mail addresses: adam0068@umn.edu (B.M. Adams), saarm@ethz.ch (M.O. Saar).

global fuel-combustion CO₂ emissions in 2017 [4]. Thus, it is likely that most fossil electricity generation will require CO₂ capture and geologic storage in saline and depleted oil and gas reservoirs to meet climate goals [5,6].

Instead of only storing CO2 in sedimentary basins as a part of CCS, the emplaced CO₂ can be circulated back to the land surface and used to generate geothermal power in a CO₂ Plume Geothermal (CPG) system [7–15]. Importantly, during CPG power generation, all of the CO₂ produced from the CO₂ storage reservoir is reinjected into the same reservoir, so that 100% of the originally injected CO2 is permanently stored underground in this CO₂ capture, utilization, and storage (CCUS) system. The use of CO₂ has many advantages over brine, such as a self-convecting thermosiphon and reduced frictional losses through the reservoir due to the decreased CO₂ viscosity [7,16]. This low CO₂ viscosity enables electric power generation from reservoirs of lower temperature and permeability than those required for traditional brine-based systems [8].

^{*} Corresponding author. Geothermal Energy and Geofluids Group, Department of Earth Sciences, ETH Zurich, Sonneggstrasse 5, 8092, Zürich, Switzerland. ** Corresponding author. Geothermal Energy and Geofluids Group, Department of

Earth Sciences, ETH Zurich, Sonneggstrasse 5, 8092, Zürich, Switzerland.

Nomenclature

D.	Mail Diameter [m]
D	Well Diameter [m]
m	Mass Flowrate [kg s ⁻¹]
P	Power [MW _e]
P_{net}	Net Power Generated at any Time, t. [MW _e]
$P_{net,avg}$	Average Net Power Generated (30 or 50 Years) [MW _e]
Q	Heat Energy Transfer Rate [MWth]
R	Reservoir Radius [m]
R_{opt}	Optimal Well Radius for Maximum Average Net
•	Power Generation [m]
t	Time [s]
T	Fluid Temperature Produced from Reservoir [°C]
T_{inj}	Fluid Temperature Injected into Reservoir [°C]
Z	Elevation [m]
Γ	Temperature Fraction [°C/°C]
δ	Reservoir Thickness [m]
К	Reservoir Permeability [m ²]
μ'	Average Reservoir Dynamic Fluid Viscosity [N s m^{-2}]

Additionally, CO₂-based geothermal power generation can leverage the fluid compressibility to provide grid-scale electricity storage [17–22]. Thus, CPG systems have increased flexibility and applicability over traditional brine-based geothermal systems.

Average Reservoir Fluid Density [kg m⁻³]

Massive amounts of thermal energy are available in the Earth's crust; however technological developments are needed to economically utilize this energy [23]. CPG can increase this geothermal energy utilization as CCS operations increase. Global CO₂ emissions exceeded 35 Gt per year in 2011 and have been rising since [1,24]. In a moderately deep (2.5 km) reservoir of moderate temperature (~100 °C) and permeability (5 \times 10 $^{-14}$ m^2), 3 MWe can be repeatedly generated by CPG from 8 Mt of permanently sequestered CO₂ [8,11]. Therefore, assuming only 10% of the global annual CO₂ emissions, currently ~35 Gt, were sequestered at comparable CPG sites, approximately 1.3 GW_e of carbon-free, baseload, and dispatchable renewable electricity could be brought online each year from geothermal resources that are unobtainable by other geothermal energy technologies [25]. This would increase the current ~14 GW_e of installed geothermal power capacity [26,27] by 9% per vear.

While research into brine-based geothermal systems is relatively extensive, CO₂ was only recently proposed as a subsurface working fluid [28,29]. Initially, CO₂ was considered only for Enhanced Geothermal Systems (EGS) [30–32], where virtually impermeable crystalline rock is hydraulically stimulated (fractured or sheared) to create flow paths for the injected CO₂ [16,33–37]. However, the nature of the fractured EGS reservoir limits its spatial extent and raises concerns such as induced seismicity [38–40].

Unlike EGS, CO₂ Plume Geothermal (CPG) utilizes sedimentary rock reservoirs, overlain by an impervious caprock. Sedimentary reservoirs have several advantages over fracture-based formations. Sedimentary reservoirs are naturally porous and permeable and are found under approximately half of the United States [41–43] and are ubiquitous worldwide [44–46]. Furthermore, the non-fracture-based flow fields that typically develop in naturally permeable sedimentary-basin reservoirs provide large specific surface areas in contact with the flowing CO₂, enabling effective heat transfer from the rock to the fluid. Lastly, saline and depleted oil and gas reservoirs in sedimentary basins are already targeted for geologic CO₂

storage [6].

Unlike traditional fracture-based systems, the heat recharge of sedimentary and EGS reservoirs is often conduction-based, rather than advection-based. As heat conduction tends to have substantially lower heat flux rates, the temperature decline of sedimentary reservoirs will be more sensitive to the heat extracted. Thus, care must be taken to select well locations and flow rates to size reservoir heat extraction sustainably.

For CO₂, thermal depletion of sedimentary basins has seldom been simulated. When heat depletion was considered, simulations included only fixed and arbitrary heat extraction rates [11,13,47,48]. As the mass flowrate of a CPG system (or any geothermal power plant) is not fixed *a priori*, but rather continually adjusted to generate the maximum power [8], only a simulator with combined reservoir, well, and surface power plant models can accurately predict the time-dependent power generation due to the associated reservoir heat depletion.

Ref. [34] account for thermal depletion in water-EGS reservoirs, employing a fixed-percentage thermal drawdown model. This is expanded in Ref. [35] by adding additional thermal drawdown models, including TOUGH2 coupling. Similarly, GETEM includes a percentage-based thermal drawdown of conventional and EGS reservoirs [49]. Despite its importance, no prior studies have simulated a complete reservoir-plant direct CO₂-based geothermal system with its varying optimum mass flowrates and heat depletion, as is done here. This has many implications, including equipment sizing, well pipe sizing, and well spacing which directly affect the cost and financial performance of a geothermal installation.

In this paper, we determine the time-dependent power generation of a direct CPG power system as the production temperature of the sedimentary basin decreases. Our earlier work [7,8] considered the power output only during the first year of operation. In addition, we calculate the effect on electricity generation by variations in reservoir thickness, permeability, well pipe diameter, and well spacing.

2. Methods

The reservoir is modeled as a truncated cylinder with a caprock above. Fig. 1 shows the radially symmetric reservoir used herein, similar to the configuration used by Ref. [11,48,50,51]. The cylindrical reservoir has a single, vertical injection well (IW) located at the center, and a continuous, horizontal circular collection well (CW) at the perimeter, directly beneath the caprock. The CO_2 is produced to the surface through four equally spaced vertical production wells (PW) which drain the collection wells. Once at the surface, the CO_2 is directly expanded through a turbine, is condensed, and then reinjected through the central injection well back into the formation.

In practice, a circular reservoir with a continuous collection well around the perimeter may not be used. CO₂ plumes tend to migrate in a preferred direction (e.g. up-dip of even slightly inclined caprocks, or along a path of higher permeability). Thus, fewer, well-placed, linear horizontal or even vertical CO₂ collection and production wells could enable circulation of most of the CO₂. However, this radially-symmetric model was chosen here as it provides computational simplicity while still allowing for simulation of the thermal depletion of a reservoir volume with buoyancy effects.

Our CPG system simulations employ two software packages: TOUGH2 [53], for subsurface simulations, and Engineering Equation Solver (EES) [54], a simultaneous equation solver with built-in thermophysical property data, for the surface plant and well piping. Ref. [51] employed a fully-coupled TOUGH2-EES reservoir and power plant simulator; however, the simulations were time-intensive

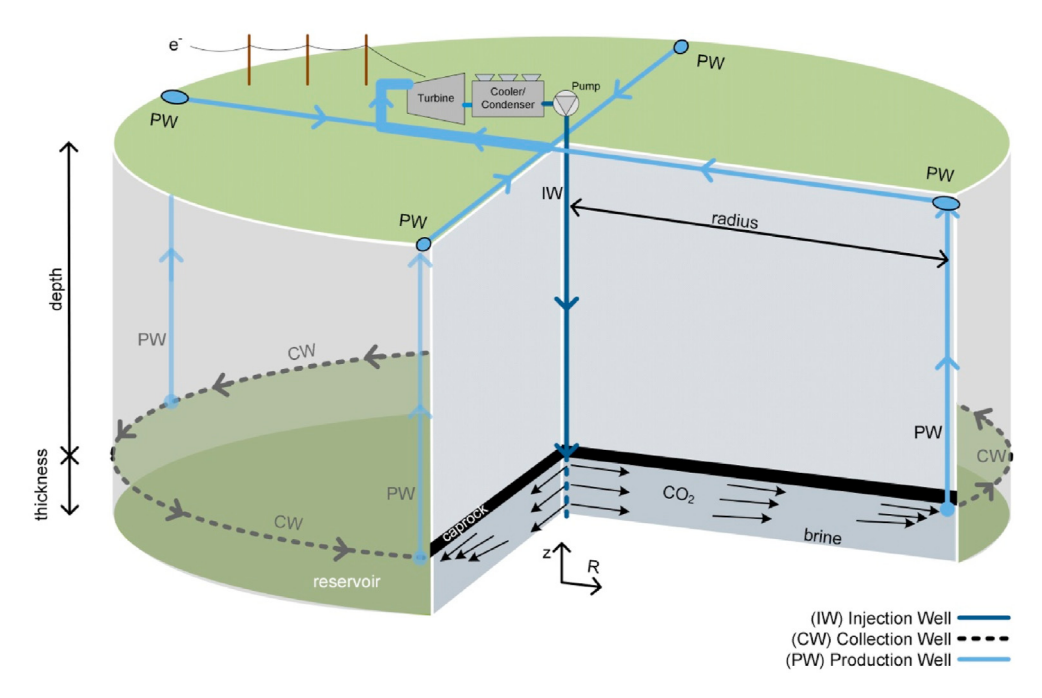


Fig. 1. Schematic of a CPG System with one central CO₂ injection well (IW) and four production wells (PW), draining an idealized horizontal, circular fluid collection well (CW) (modified from Ref. [52]. None of the injected and circulated CO₂ is released to the atmosphere.

as repeated TOUGH2 simulations with slightly different mass flowrates were required. Additionally, Ref. [51] did not consider the thermal depletion of a reservoir, which would have made simulation time even longer.

To reduce computational time in this study, the TOUGH2 simulator results are characterized by the relevant system parameters (i.e. depth, temperature gradient, permeability, radius, and CO₂ injection fluid state) into a set of dimensionless curves, which are then integrated into the EES simulator. Thus, we consider the subsurface, wells, and power plant as a single system.

The time-dependent power generation of the CPG system is found for various combinations of the parameters listed in Table 1. The 'Varied' reservoir conditions are the parameters which are modified in the results section of this paper. The 'Not Varied' reservoir conditions are the values used in all TOUGH2 reservoir simulations. The reservoir properties are chosen to be consistent with our previous work and models [11,51]. All power plant parameters are identical to Ref. [8]. The well pipe diameters are derived from GETEM [55]. The reservoir parameters were originally chosen to be representative of typical sedimentary basins available for deep geothermal and their associated surface power plants.

Section 2.1 characterizes the TOUGH2 simulator for integration

Table 1Parameters used.

Well Pipe Diameter	0.14 m, 0.27 m, 0.33 m, and/or 0.41 m								
Reservoir Parameters: Varied									
Depth	1.5 km, 2.5 km, 3.5 km, or 5.0 km								
Thickness	50 m or 300 m								
Radius	300 m or 707 m								
Geothermal Gradient	20 °C km $^{-1}$, 35 °C km $^{-1}$, or 50 °C km $^{-1}$								
Permeability	$1 \times 10^{-12} \text{ m}^2$ to $1 \times 10^{-15} \text{ m}^2$								
Reservoir Parameters: Not Varied									
Rock Density	2300 kg m^{-3}								
Rock Specific Heat	$0.92 \text{ kJ kg}^{-1} \text{ C}^{-1}$								
Rock Thermal Conductivity	$2.1 \text{ W m}^{-1} \text{ C}^{-1}$								
Porosity	0.10								
Reservoir Fluid	CO ₂ injected into 20 wt% NaCl-brine								
CO ₂ Injected Initially	2 to 10 Mt CO ₂ (See Ref. [11])								

into the EES simulator. Section 2.2 describes the EES simulator, which calculates power generation, using the characterization of Section 2.1. shows our nomenclature.

2.1. Reservoir modeling and characterization

The reservoir is considered to be homogeneous, horizontal, and radially symmetric; initially at uniform temperature and pressure. The reservoir is modeled using TOUGH2 [53] with the ECO2N and ECO2H equation of state modules [53,56,57]. The reservoir parameters are described in Table 1.

The initial temperature of the reservoir is the product of the geothermal temperature gradient and reservoir depth plus the average ambient air temperature (15 °C). A 15 °C average air temperature is a cautious assumption, representative of Dallas, TX, U.S [8]. The initial pressure is the hydrostatic elevation potential of pure water at the given depth. The injection well is vertical and centrally located (R=0). The grid spacing in the reservoir increases with radial distance, up to the radial extent of the reservoir (100 km) to account for brine displacement, thermal expansion, and overpressurization, which occur from CO₂ injection [11,48,50]. The horizontal and circular collection well (CW) is located directly beneath the impermeable caprock, at a radial distance, R, from the vertical injection well. The radially-symmetric nature of the reservoir model assumes a uniform pressure in the horizontal collection wells. This is justifiable as the flowrates in the horizontal wells are at most half of the production well flowrate and at least, zero flowrate. Similarly, it was found that a single vertical production well substantially limits power generation due to high frictional losses. Thus, four vertical production wells, operating in parallel, are considered (see CW and PW in Fig. 1).

The reservoir initially contains 20 wt% NaCl-brine. Then, pure CO₂ is injected, first without fluid production, partially displacing the brine over approximately 2 years. Fluid production commences once a minimum CO₂ mass-fraction of 94% is achieved into the production well [58], which is consistent with previous publications [11]. However, recent discussions with turbine manufacturers

indicate that much lower CO₂ mass fractions are permissible within the turbine without damaging it.

The injection temperature of CO_2 back into the reservoir, T_{inj} , is determined by isentropically compressing saturated liquid CO_2 to the hydrostatic pressure at reservoir depth. The saturated liquid CO_2 is at ambient temperature plus a 7 °C approach temperature as it leaves the condensing tower (i.e. 22 °C). Thus, the reservoir injection temperatures are 35, 46, 58, and 65 °C for depths of 1.5, 2.5, 3.5, and 5.0 km, respectively.

The reservoir produced fluid temperature is simulated for CO_2 injection mass flowrates of 3 (95.1), 4 (126.8), 5 (158.5), and 6 Mt yr⁻¹ (190.2 kg s⁻¹), initially ramping linearly from zero to the specified mass flowrate over the first two years, and continuing for a minimum of 50 years. To increase the TOUGH2 simulation reliability, an increased number of parameters are used: reservoir thicknesses of 50, 100, 200, and 300 m, injection-to-production well radii of 300, 500, 707, 1000, 1200, 1500, 2000, and 2500 m, at reservoir depths of 1.5, 2.5, 3.5, and 5.0 km, and geologic thermal gradients of 35 and 50 °C km⁻¹, although not all combinations are simulated. The temperature decay is non-dimensionalized into the temperature fraction, Γ , where T(t) is the downhole production well temperature at time t (Equation (1)).

$$\Gamma(t) = \frac{T(t) - T_{inj}}{T(0) - T_{inj}} \tag{1}$$

A permeability of $5\times 10^{-14}~\text{m}^2$ is used for all simulations as previous work has shown that reservoir impedances can be reliably adjusted from a base case for any permeability by applying Darcy's Law [8]. The reservoir impedance (i.e. 'reservoir factor, *R*' in Ref. [8] is the fluid pressure difference between reservoir fluid injection and production pressures divided by the fluid mass flowrate. The reservoir fluid pressures are non-dimensionally scaled using a correction factor from the analytical Darcy reservoir impedance solution, given in Equation (2). Ref. [52] provides this correction factor to obtain the two-phase, time-dependent value, which is used herein.

$$\frac{P_{ideal}}{m'} = \left(\frac{\mu'}{\rho'}\right) \frac{1}{2\pi\kappa\delta} ln\left(\frac{2R}{D}\right)$$
 (2)

The resulting 330 TOUGH2 reservoir simulation datasets are analyzed to construct response curves for the investigated system. This enables estimation of reservoir impedance and thermal decay in the reservoir for a given set of input parameters at a given time step without the need to run further simulations. Specifically, the temperature decay profile of a sedimentary reservoir is approximated using a two-variable error function and exponential combination curve across the parameter space. On average, the combined error function and exponential curve fit the 330 individual datasets well ($r^2=0.989$). The derivation of the response curves for reservoir impedance and thermal decay is detailed in Ref. [52]. The derived response curves are used in the following section of this work to compute the produced heat flux and electric power generation with time.

2.2. Surface power plant modeling

The surface power plant converts the geothermal heat to electric power. The plant includes production and injection well piping, a direct-CO₂ turbine, cooler, condenser, and a surface injection pump, as shown in Fig. 2. The surface power plant is identical to that used previously [8]. Engineering Equation Solver (EES) is used to solve for CO₂ fluid properties, based on Ref. [59].

Saturated liquid CO_2 at a temperature equal to ambient plus a 7 °C approach temperature (22 °C) leaves the surface condenser

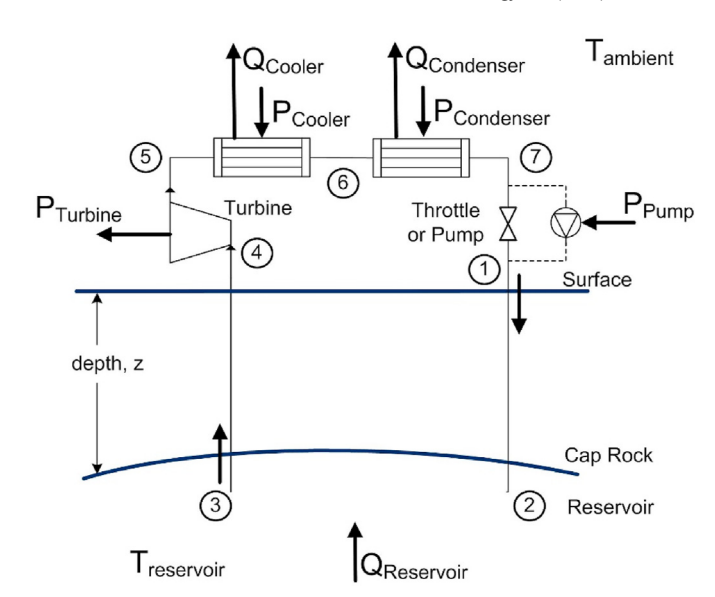


Fig. 2. Direct CPG system schematic (modified from Ref. [8]. The CPG system mass flowrate is optimized to generate the most power for the specific reservoir characteristics. This involves either throttling or pumping the system as the downhole injection well pressure requires.

(State 7). The CO₂ is either throttled or pumped to the requisite pressure at State 1, which will maintain the pressure of State 3 at hydrostatic. The CO₂ is injected at the surface into the injection well, where it self-compresses into supercritical CO₂ before entering the reservoir at State 2. The CO₂ flows through the reservoir, increasing in temperature and decreasing in pressure to State 3, where the pressure is hydrostatic. The pressure change within the reservoir is the product of the reservoir impedance and fluid mass flowrate. The CO₂ then flows isobarically through the horizontal circular collection well and with decreasing pressure up the production wells to the surface (State 4). Wellbore heat loss is low at high flowrates and thus neglected [60,61]. At the surface, the CO₂ expands through a turbine with an isentropic efficiency of 78% to State 5. It is isobarically de-superheated in a cooler to State 6, and then isobarically condensed to State 7 at a pressure equivalent to the saturation pressure of CO₂ at 22 °C.

Pure CO₂ is assumed within the wellbores and equipment; however, the power generation would be larger if water-saturated CO₂ from the reservoir entered the production well [10]. The effect of multicomponent fluid (CO₂ and water) flow on power generation and liquid loading potentials in CPG production wells are investigated in Ref. [58].

For every combination of well pipe diameter, injection-to-production well radius, reservoir permeability, and reservoir thickness, the net power is found in 5-year increments from Years 0–50. At each time step, the reservoir produced fluid temperature and pressure differential are recalculated using the fits described in Section 2.1 (see also [8]). At each time step, the CPG system is operated at the mass flowrate that provides the largest net power (see Figure 4 in Ref. [8]). Turbine power generated, net power, and parasitic loads are calculated identically to Ref. [8].

3. Results and discussion

The net power generated is found for each of the parameter combinations (Table 1). Fig. 3 shows the time-series of A) net power, B) temperature fraction, and C) mass flowrate for a 2.5 km deep, $35 \,^{\circ}$ C km⁻¹ temperature gradient, and 5×10^{-14} m² reservoir permeability with 0.41 m pipe diameter injection and production

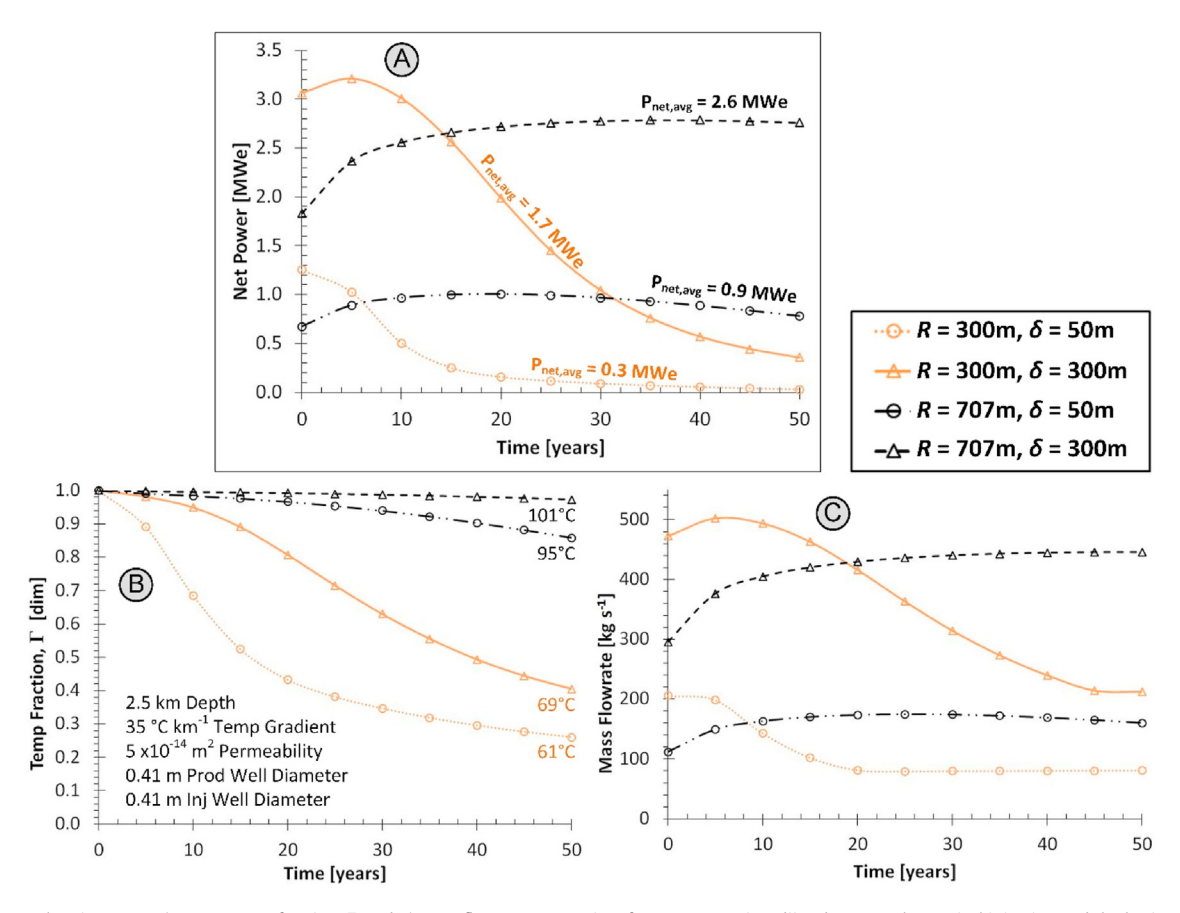


Fig. 3. The A) net electric power, B) temperature fraction, Γ , and C) mass flowrate versus time for two reservoir radii, R, between the vertical injection and the horizontal collection well, and two reservoir thicknesses, δ. These values are shown for a 2.5 km deep reservoir with a 35 °C km⁻¹ temperature gradient (plus 15 °C average ambient air temperature), 5×10^{-14} m² permeability, and 0.41 m pipe diameter injection, collection, and production wells. Fig. 3B shows the equivalent reservoir production temperature after 50 years.

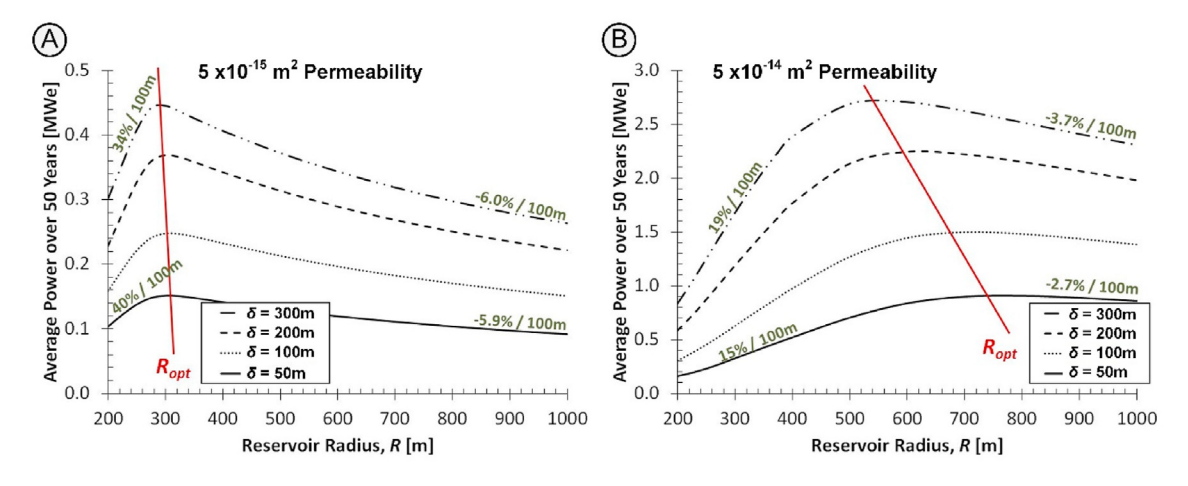


Fig. 4. The average net electric power over 50 years as a function of reservoir radius, R, between the vertical injection well and the horizontal, circular collection well, for four reservoir thicknesses at a permeability of A) 5×10^{-15} m² and B) 5×10^{-14} m². The reservoirs are identical otherwise, with a 2.5 km depth, 35 °C km⁻¹ temperature gradient plus 15 °C ambient air temperature, and 0.41 m well pipe diameters. The red line indicates the trend of optimum radii, R_{opt} , across reservoir thicknesses, δ . The slopes of the power curves, approximated as linear on either side of the maximum, are provided for reservoir thicknesses of 50 and 300 m. The power slopes are given in units of percentage change per 100 m radius change, where the percentage change is the power slope divided by the maximum average power value for that reservoir thickness and permeability. (For interpretation of the references to color in this figure legend, the reader is referred to the Web version of this article.)

wells.

Fig. 3A shows that increasing the reservoir thickness, δ , always increases the maximum net power generation. This is due to the inverse relationship between reservoir thickness and fluid pressure differential in the Darcy equation (Equation (2)): increasing the

reservoir thickness decreases the reservoir impedance and thus increases the fluid mass flowrate and net power. In the same way, decreasing the reservoir radius decreases the reservoir impedance, though this effect is small at large radii. However, a decrease in reservoir impedance, while increasing mass flowrate and

instantaneous net power, also decreases the time to thermal breakthrough at the production well. Thus, while the 300 m radius reservoirs in Fig. 3A have a larger maximum power than the 707 m reservoirs, they have lower average power values. Therefore, for any given reservoir impedance, there will be a radius, R_{opt} , which provides the maximum average net power over a given time period, explained further in Section 3.1.

For each reservoir configuration, the maximum mass flowrate (Fig. 3C) occurs at non-zero time. This maximum is caused by the interactions between reservoir impedance and production temperature. As the reservoir "dries out" with time (larger fractions of the pore space are occupied by CO₂ and fewer by brine), its impedance decreases, and the fluid pressure differential created by the thermosiphon induces a greater mass flowrate, all else staying constant. In contrast, the reservoir downhole production temperature (Fig. 3B) decreases with time, which decreases the density differential between injection and production wells, and would decrease thermosiphon-induced mass flowrate, all else remaining constant [7]. Thus, for systems with rapid thermal drawdown (e.g. for a shorter 300 m radius), the decreasing reservoir impedance is quickly counter-acted by the decreasing production temperature, vielding earlier maximum mass flowrates. Similarly, systems with greater reservoir radii have larger thermal masses, so that production temperatures decrease more slowly and mass flowrates peak later.

Lastly, Fig. 3 shows that at large thermal depletion (i.e. small temperature fraction), the optimal mass flowrate reaches a horizontal asymptote. This asymptote is the thermosiphon-driven mass flowrate that results without pumping. When the production temperature becomes sufficiently low, it no longer generates more electricity to augment the system mass flowrate with pumping. However, there is also no benefit to throttling the system to lower mass flowrates. Thus, a steady mass flowrate is obtained.

3.1. Optimal radius, R_{opt} , for given reservoir thickness

For any given reservoir thickness, the optimal radius, R_{opt} , between the vertical injection well and the horizontal, circular collection well, is the radius which will produce the greatest average net power over the lifetime of the reservoir. To more clearly define this optimum radius, additional simulations are run for 50 years of operation for a reservoir depth of 2.5 km, a geothermal temperature gradient of 35 °C km $^{-1}$ plus 15 °C ambient air temperature, permeabilities of 5×10^{-15} and 5×10^{-14} m 2 , thicknesses, δ , of 50, 100, 200, and 300 m, and radii between 200 and 1000 m. The results are shown in Fig. 4.

In all cases, for a given reservoir radius, increasing the reservoir thickness yields increased power. For each of the thicknesses shown in Fig. 4, a maximum average net power is obtained within the radius range of 200–1000 m. Described previously, the optimum radius occurs due to the interaction between the differential pressure and thermal mass, which affect the average net power generation in opposing ways. For a permeability of 5×10^{-14} m² (Fig. 4B), the optimum radii are near 550 and 750 m for reservoir thicknesses of 300 and 50 m, respectively.

The red line in Fig. 4 shows the trend of maximum power across reservoir thicknesses. It has a negative slope, indicating a decreased optimum reservoir radius for increasing reservoir thicknesses. The optimum radius is larger for thinner reservoirs to counter the reduction in thermal mass that occurs through decreasing reservoir volume. For a permeability of 5×10^{-15} m² (Fig. 4A), the red line is nearly vertical, with an optimal radius of ~300 m for all investigated reservoir thicknesses. For low permeabilities, the mass flowrate is very sensitive to radius so that the penalty incurred for undersizing or over-sizing the reservoir radius is much larger than for

higher permeabilities.

For a given reservoir thickness, the approximate linearized slopes of the power curves (gray power curves) in Fig. 4 indicate the energy penalty for an incorrect radius choice. The linearized slope is the change in power generation for a 100 m radius change divided by the maximum power generated (% per 100 m) for that reservoir thickness. For example, for a 5×10^{-15} m² permeability reservoir (Fig. 4A) with a thickness of 300 m, 6% of the maximum power is lost for every 100 m of over-sizing. Thus, placing a production well at 600 m instead of 300 m will decrease power by approximately 18% of peak power (90 kW_e).

The magnitude of the power slope tends to be larger for undersized radii than oversized radii. Thus, an oversized reservoir radius impacts the average power generation less over the lifetime of the system than selecting a radius that is too small. Additionally, as reservoir permeabilities increase (from Fig. 4A and B), the power slopes decrease, indicating that the selection of a correctly sized production well radius is more important for low reservoir permeabilities.

The optimum reservoir radius, R_{opt} , will vary depending on the time period over which the maximum average power is sought. For decreased time periods (e.g. 30 instead of 50 years), the thermal energy required to be extracted decreases, decreasing the required reservoir radius. Thus, for decreasing CPG lifetimes of interest, the optimum radius decreases, causing the average power generation to increase.

3.2. Average net power variability across the parameter space

The average net electric power generation values are found for each parameter (Table 1) and a subset are displayed in Fig. 5 with fixed injection and production well pipe diameters of 0.41 m. The values are colored to indicate low (red), intermediate (yellow), and high (green) values of net power generation. As power output was previously found to be negligible for reservoir depths less than 3.5 km at a temperature gradient of 20 °C km⁻¹ and less than 2.5 km at a temperature gradient of 35 °C km⁻¹ [62], those values are not simulated and are represented as blank cells. For comparison, the parameter combinations that yield larger CPG power generation values than using brine in Ref. [8] (see their Figure 7) are bordered by a dark black line. This is shown only for the combinations with 300 m thickness reservoirs and 707 m reservoir radii, which most closely align with that study.

Consistent with previous findings, the average power increases with increases in reservoir depth and permeability as well as temperature gradient. For fixed values of reservoir depth, permeability, reservoir radius, and temperature gradient, increasing the reservoir thickness results in an increase in power generated.

These results may be compared to those of the pure- CO_2 inverted 5-spot reservoir of Ref. [8] using the 300 m thickness and 707 m radius reservoir values. For injection and production well pipe diameters of 0.41 m, a reservoir permeability of 5×10^{-14} m², temperature gradient of $35\,^{\circ}$ C km $^{-1}$, and depth of 2.5 km, Ref. [8] in their Figure 6A reported a net power of 3.6 MW_e, which can be compared to 2.6 MW_e here. The difference (-32%) can be attributed to the higher reservoir impedance of the more realistic multi-phase reservoir considered here, which is initially filled with brine. Also, the power shown here can be improved upon; it increases slightly from 2.6 MW_e to 2.7 MW_e (or +4%) by decreasing the collection well radius from 707 to 600 m (Fig. 4B).

As previously discussed, power does not necessarily increase with reservoir radius, although this tends to occur for the two radii (300 and 707 m) shown in Fig. 5, especially at high permeabilities. For permeabilities of 5 \times 10 $^{-14}$ m² and larger, a radius of 707 m results in more average power than using a 300 m radius; however,

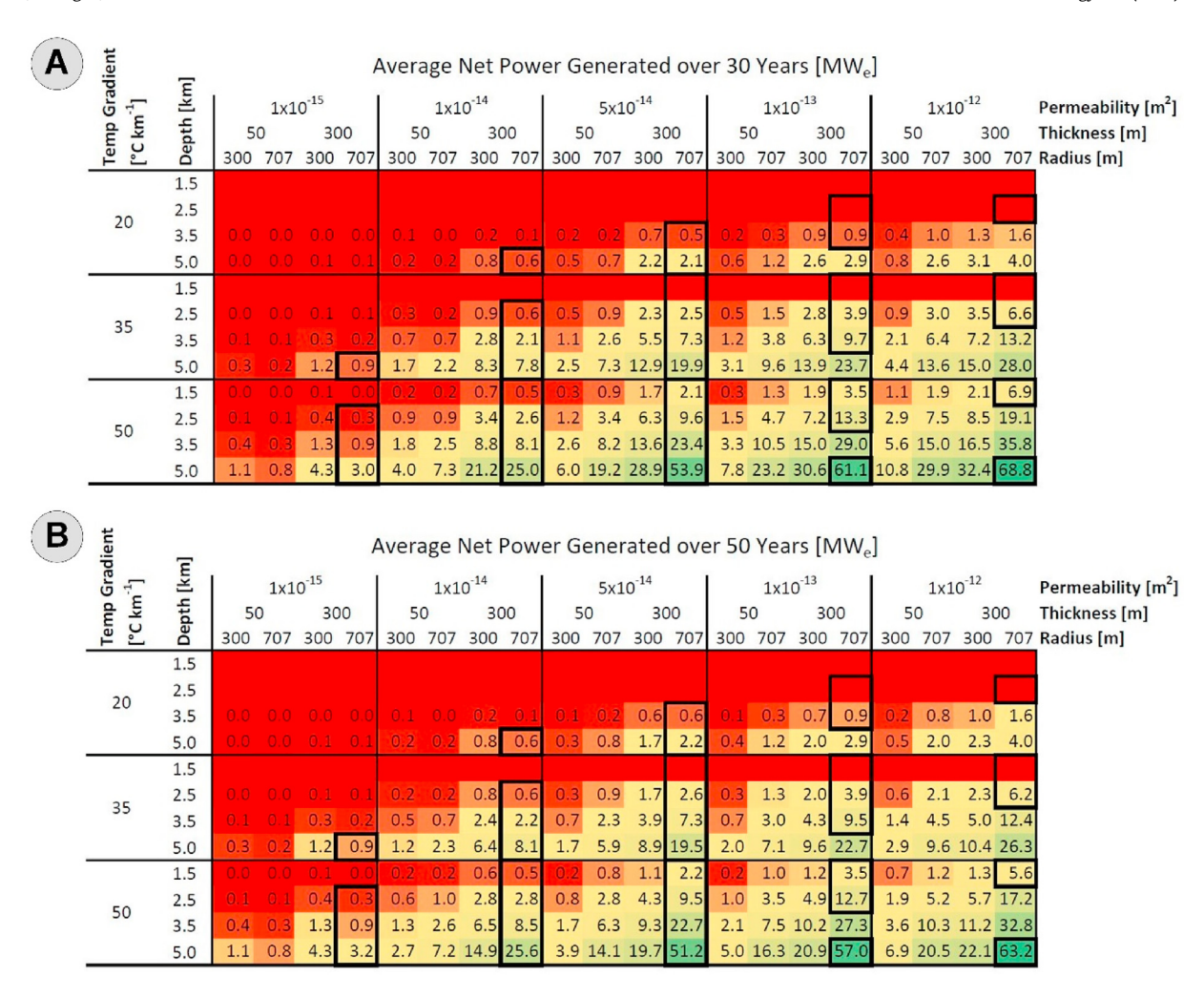


Fig. 5. The average net electric power generated over the first A) 30 years and B) 50 years for selected values of reservoir permeability, thickness, radius, depth, and temperature gradient with a fixed well pipe diameter of 0.41 m. Permeability, depth, and temperature gradient combinations are outlined in bold which were previously shown to yield higher power generation rates than brine-based geothermal systems (see Ref. [8]).

	Temp Gradient [°C km ⁻¹]	_	Percent Change in Power, $\Delta P_{net,avg}$																				
(_ - Gra	[km]	1x10 ⁻¹⁵				1x10 ⁻¹⁴					5x1	0 ⁻¹⁴			1x1	0 ⁻¹³	8	1x10 ⁻¹²				Permeability [m ²]
m kr		Depth	50 300		0	50		300		50		30	300		50		300		50		00	Thickness [m]	
	Tel [°C	De	300	707	300	707	300	707	300	707	300	707	300	707	300	707	300	707	300	707	300	707	Radius [m]
20		1.5																					
	20	2.5																					
	20	3.5							-2	-6	33	-6	14	-5	57	-2	24	-3	47	23	31	1	
		5.0					7	-6	2	-6	43	-2	27	-3	48	7	32	-1	53	30	35	2	
35		1.5																					
	25	2.5					20	-6	5	-6	49	3	39	-4	57	18	44	0	57	45	53	6	
	33	3.5			-2	-6	32	-6	17	-6	49	12	42	-1	57	27	44	2	53	42	44	6	
		5.0	-1	-6	-1	-6	41	-4	31	-4	52	24	44	2	53	36	45	4	55	43	45	6	
5	<u> </u>	1.5					35	-6	15	-6	57	8	57	-4	57	34	57	1	57	57	57	24	
	50	2.5	-2		-2	-6	39	-6	23	-6	51	20	46	0	56	36	47	5	57	46	49	11	
	30	3.5	-2	-6	-2	-6	43	-3	34	-5	52	29	47	3	57	40	47	6	56	46	47	9	
		5.0	0	-6	-1	-6	47	1	42	-3	54	37	47	5	55	43	47	7	56	45	47	9	

Fig. 6. The percent change in average net electric power generated when a 30-year average is used instead of a 50-year average. Positive changes are indicated by green while negative changes are shown in red. Large positive changes (green) between 50- and 30-year averages indicate a substantially heat-depleted reservoir at the 30-year mark, while negative changes (red) indicate thermal breakthrough has not yet occurred and, in fact, that power generation is still increasing due to continued reductions in reservoir impedance. (For interpretation of the references to color in this figure legend, the reader is referred to the Web version of this article.)

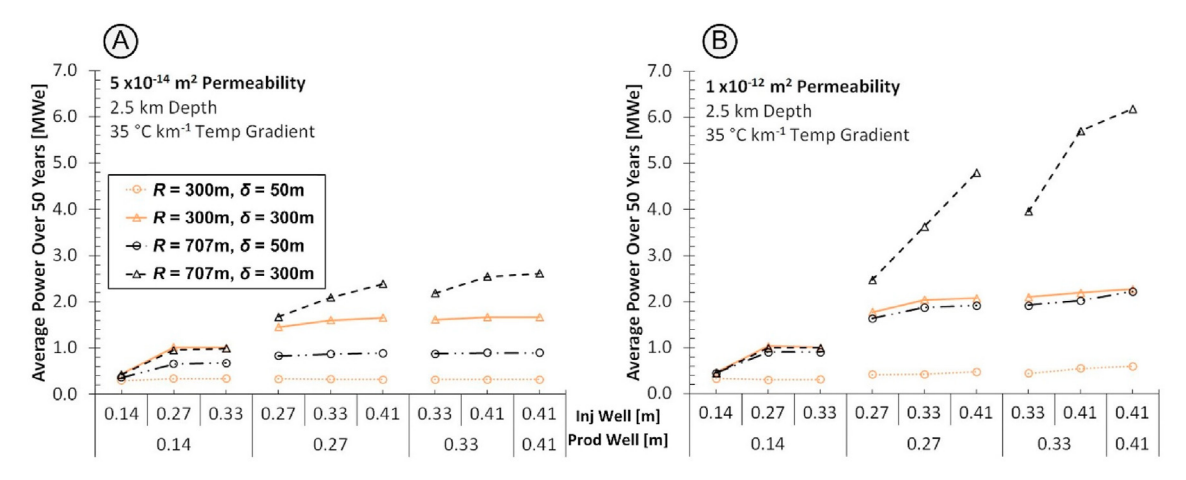


Fig. 7. The average net electric power generated over 50 years for varying well pipe diameters for A) a 5×10^{-14} m² permeability reservoir and B) a 1×10^{-12} m² permeability reservoir. The reservoirs are 2.5 km deep and have thicknesses, δ, of 50 and 300 m. The geologic temperature gradient is 35 °C km⁻¹, while the average ambient air temperature is 15 °C (resulting in a reservoir temperature of 102.5 °C). The reservoir radii, R, indicating the distance between the vertical injection well and the horizontal collection well, are 300 and 707 m.

at low permeabilities, especially those at shallow depths and low temperatures, the power output with a radius of 707 m can be lower than that at 300 m.

To determine if the reservoirs examined were sized correctly, the change in power generated between 30-year and 50-year averaging windows is found. The percent change in power, $P_{net,avg}$, is the difference between the average net power generated over 30 years, $P_{net,avg,30y}$, and 50 years, $P_{net,avg,50y}$, divided by the average net power generated over 30 years, given in Equation (3).

$$\Delta P_{net,avg} = \frac{P_{net,avg,30y} - P_{net,avg,50y}}{P_{net,avg,30y}} \times 100\%$$
 (3)

The results are shown in Fig. 6, where large, positive percentage changes (green) indicate an undersized reservoir radius, *R*, with too little reservoir thermal mass, causing thermal breakthrough at the production well between Years 30 and 50. The thermal breakthrough results in the reservoir operating at a fraction of its peak power generation toward the end of its 50-year lifetime, causing a decrease in average power generated. In the cases with large positive values (e.g. most 300 m radius cases), the production wells should be placed at a larger radius from the injection well, *R*, to increase the thermal mass through which the heat extraction fluid flows.

In contrast, negative changes in power (red) indicate that the net power is continuing to rise beyond 30 years. In these cases, thermal breakthrough has not yet occurred, and continued decreases in the reservoir impedance with time, due to larger $\rm CO_2$ saturations of the pore space, cause increased mass flowrate and net power output (e.g. the 707 m radius and 300 m thickness reservoir in Fig. 3). Thus, reservoir thicknesses and CPG well combinations shown in Fig. 6 with single-digit change magnitudes are sized appropriately to provide consistent power for a 50 year duration.

From Fig. 6, we can infer that a 300 m thickness reservoir with a 707 m radius well spacing will not substantially deplete in heat for any of the reservoir combinations shown over a 50-year lifetime; however, improved performance may be found at smaller radii, as previously discussed. Also, at low permeabilities, such as 10^{-14} m², a reservoir with a 707 m radius well spacing does not deplete in heat for either a 50 m or 300 m thickness, while none of the reservoir thicknesses and radii considered deplete in heat over 50 years in a 10^{-15} m² permeability reservoir.

3.3. Average net power sensitivity to well pipe diameter

The effect of well pipe diameter on average net power is shown in Fig. 7 for both a 5×10^{-14} m 2 and 1×10^{-12} m 2 permeability reservoir at a depth of 2.5 km, a 35 °C km $^{-1}$ geologic temperature gradient, and a range of well pipe diameters. Well pipe diameter and reservoir permeability govern the system pressure losses, which dictate the mass flowrate that will generate the most power.

When increasing injection and production well pipe diameter, the average electric net power tends to increase. Likewise, increases in reservoir permeability tend to increase the power generated; however, this effect is diminished at small pipe diameters. At large reservoir permeabilities (Fig. 7B), the fraction of frictional pressure losses from the reservoir tends to be low; therefore, net power output is substantially increased by increasing well pipe diameter. Conversely, at low reservoir permeabilities (Fig. 7A) the fraction of frictional pressure losses from the reservoir is large, so the net power output is less sensitive to the pipe diameter.

For each combination of reservoir radius, R, and reservoir thickness, δ , there appears to be a combination of injection and production well pipe diameters, where a plateau in net power generation is achieved. The exception to this trend is the 707 m reservoir radius and 300 m reservoir thickness case in Fig. 7B, where power increases for all increases in pipe diameter. These results notably differ from those previously found (see Figure 10A in Ref. [8], which indicated that power increased for all increases in pipe diameter. Ref. [8] did not consider the temperature depletion that occurs with time and its effect on power generation.

Fig. 7 shows that for all but the largest reservoir (i.e. reservoir radius of 707 m and thickness of 300 m), the average power does not increase appreciably for injection and production well pipe diameters greater than 0.27 m. This is caused by the rapid thermal depletion of the reservoir that larger pipe diameters enable. While the average power generation for different well pipe diameter combinations is roughly equivalent, larger pipe diameters provide variability in power generation with time. Conversely, the 707 m radius and 300 m thickness reservoir does not thermally deplete for large values of pipe diameter, as previously indicated in Fig. 6. Thus, for a fixed reservoir volume, the wells need to be sized accordingly to avoid installation of unnecessarily large piping.

Further, the correct sizing of well pipe diameters will decrease the net power variation with time, decrease the over-sizing of power plant equipment, increase the capacity factor of that equipment, and overall decrease the cost of generating electricity. This result is consistent with Ref. [58] which similarly shows that the largest well pipe diameters may not be the optimum design choice, but for reasons of wellbore flooding.

Ultimately, considerations regarding the site-specific reservoir characteristics (permeability, thickness, etc.), the anticipated engineered subsurface features (well and well-field geometries), and Earth surface conditions (CO₂ sources or pipelines, power users or power grid proximity, average air or surface-water temperature for cooling, etc.) all need to be included when implementing CPG power generation and associated permanent geologic CO₂ storage. In practice, a wide range of in-depth simulations of combined reservoir-power-plant processes and their uncertainties (particularly regarding the uncertain subsurface parameters, the uncertainty of which can be reduced through geological/geophysical exploration) will have to be conducted for each potential CPG site. Such simulations provide forecasts of CPG system implementations for a site of interest, yielding estimated power output and associated revenue, costs, and mass of permanently stored CO2 for many decades into the future of a potential CPG system's operation time. Nonetheless, we hope that the insights provided here can provide guidance when pre-screening locations for potential CPG system development.

4. Conclusions

In this paper, we use fluid pressure drop and temperature decay characterizations of sedimentary radial reservoirs from Ref. [52] to find the time-dependent values of CPG power generation for various well pipe diameters, reservoir radii, thicknesses, and permeabilities. Our findings are:

- A given reservoir has an optimal reservoir radius, R_{opt}, that maximizes average power generation over a specified time. The reservoir radius is determined by the well spacing and placement. Increasing the reservoir radius increases both the reservoir impedance and the reservoir thermal mass available for heat extraction, as large-radii reservoirs yield lower flowrates and thus slower heat depletion. Additionally, this optimum radius increases with increasing reservoir permeability.
- For 300 m thick reservoirs, the 707 m reservoir radius, R, provides sufficient heat to sustain power generation over a 50-year period. The change in average power generation between 30- and 50-years is almost always less than 10%, indicating consistent power output and low heat depletion. For 50 m thick reservoirs, the change in power generation for this spacing is generally less than 25% for permeabilities of 5×10^{-14} m² and below.
- Over-estimation of the reservoir radius, R, affects the long-term power output less severely than under-estimation. Additionally, power sensitivity to reservoir radius is more pronounced for smaller than for larger permeabilities.
- Increasing injection and production well pipe diameter for a fixed reservoir radius, R, does not necessarily increase average net power generation. While increasing well pipe diameters increases mass flowrate and therefore net power generation, an increased pipe diameter also increases heat extraction from the reservoir, leading to faster heat depletion. A moderation of the heat extraction rate also decreases the required capacity of the surface plant while increasing equipment capacity utilization over time, thus reducing cost of generation.
- Larger reservoir thicknesses increase the average power generated.
 All else constant, larger reservoir thicknesses increase the flow-cross-sectional area, decrease the reservoir impedance, and result in higher flowrates, while the thermal mass of the reservoir is increased.

Data availability

The power generation data for all cases simulated are provided as supplemental data as an EXCEL file.

CRediT authorship contribution statement

Benjamin M. Adams: Conceptualization, Methodology, Software, Data curation, Formal analysis, Writing - original draft. Daniel Vogler: Writing - review & editing. Thomas H. Kuehn: Conceptualization, Writing - review & editing, Supervision, Funding acquisition. Jeffrey M. Bielicki: Conceptualization, Writing - review & editing, Funding acquisition. Nagasree Garapati: Data curation, Writing - review & editing, Martin O. Saar: Conceptualization, Writing - review & editing, Supervision, Funding acquisition.

Declaration of competing interest

The authors declare that they have no known competing financial interests or personal relationships that could have appeared to influence the work reported in this paper.

Acknowledgements

The authors gratefully acknowledge funding from a U.S. National Science Foundation (NSF) Sustainable Energy Pathways (SEP) program grant (1230691). We also thank the Initiative for Renewable Energy (IREE) for initial seed funding. The Werner Siemens Foundation (Werner Siemens-Stiftung) is further thanked for its support of the Geothermal Energy and Geofluids (GEG.ethz.ch) Group at ETH Zurich. We acknowledge additional funding from: the U.S. National Science Foundation Innovations at the Nexus of Food, Energy, and Water Systems (INFEWS) program (1739909), the U.S. National Science Foundation National Research Traineeship Program (1922666), and the Sloan Foundation. We also thank our two peer reviewers for their thoughtful feedback. Any opinions, findings, conclusions, and/or recommendations expressed in this material are those of the authors and do not necessarily reflect the views of the NSF, IREE, UMN, OSU, or ETH.

References

- [1] Intergovernmental Panel on Climate Change (IPCC), Climate Change 2014: Synthesis Report, 2014. http://www.ipcc.ch/report/ar5/syr/.
- [2] Intergovernmental Panel on Climate Change (IPCC), IPCC special report on carbon dioxide capture and storage, in: B, Metz, O. Davidson, H.C. de Coninck, M. Loos, L.A. Meyer (Eds.), Prepared by Working Group III of the Intergovernmental Panel on Climate Change, Cambridge University Press, 2005. https://www.ipcc.ch/report/carbon-dioxide-capture-and-storage/.
- [3] Intergovernmental Panel on Climate Change (IPCC), Global warming of 1.5°C: an IPCC special report on the impacts of global warming of 1.5°C above preindustrial levels and related global greenhouse gas emission pathways, in: P. Zhai, H.-O. Pörtner, D. Roberts, J. Skea, P.R. Shukla, A. Pirani, W. Moufouma-Okia, C. Péan, R. Pidcock, S. Connors, J.B.R. Matthews, Y. Chen, X. Zhou, M.I. Gomis, E. Lonnoy, T. Maycock, M. Tignor, T. Waterfield (Eds.), The Context of Strengthening the Global Response to the Threat of Climate Change, Sustainable Development, and Efforts to Eradicate Poverty [Masson-Delmotte, 2018, https://www.ipcc.ch/sr15.
- [4] International Energy Agency (IEA), CO2 Emissions from Fuel Combustion 2019
 Edition. https://www.iea.org/data-and-statistics/?country=WORLD&
 fuel=CO2+emissions, 2019.
- [5] C. Azar, K. Lindgren, E. Larson, K. Möllersten, Carbon capture and storage from fossil fuels and biomass—Costs and potential role in stabilizing the atmosphere, Climatic Change 74 (2006) 47–79.
- [6] Global CCS Institute, The Global Status of CCS: 2019—Targeting Climate Change, 2019. http://www.globalccsinstitute.com/resources/global-status-report.
- [7] B.M. Adams, T.H. Kuehn, J.M. Bielicki, J.B. Randolph, M.O. Saar, On the importance of the thermosiphon effect in CPG (CO₂ plume geothermal) power systems, Energy 69 (2014) 409–418, https://doi.org/10.1016/

- j.energy.2014.03.032.
- [8] B.M. Adams, T.H. Kuehn, J.M. Bielicki, J.B. Randolph, M.O. Saar, A comparison of electric power output of CO₂ Plume Geothermal (CPG) and brine geothermal systems for varying reservoir conditions, Appl. Energy 140 (2015) 365–377, https://doi.org/10.1016/j.apenergy.2014.11.043.
- [9] J. Ezekiel, A. Ebigbo, B.M. Adams, M.O. Saar, Combining natural gas recovery and CO₂-based geothermal energy extraction for electric power generation, (2020) 269 115012, https://doi.org/10.1016/ Energy apenenergy.2020.115012.
- [10] M.R. Fleming, B.M. Adams, T.H. Kuehn, J.M. Bielicki, M.O. Saar, Increased power generation due to exothermic water exsolution in CO2 Plume Geothermal (CPG) power plants, Geothermics 88 (2020) 101865, https://doi.org/10.1016/ geothermics.2020.101865.
- [11] N. Garapati, J.B. Randolph, M.O. Saar, Brine displacement by CO₂, energy extraction rates, and lifespan of a CO₂-limited CO₂-Plume Geothermal (CPG) system with a horizontal production well, Geothermics 55 (2015) 182–194, https://doi.org/10.1016/j.geothermics.2015.02.005.
- [12] J.B. Randolph, M.O. Saar, Coupling geothermal energy capture with carbon dioxide sequestration in naturally permeable, porous geologic formations: a comparison with enhanced geothermal systems, Trans. Geoth. Resour. Counc. 34 (2010) 433-437
- [13] J.B. Randolph, M.O. Saar, Combining geothermal energy capture with geologic carbon dioxide sequestration, Geophys. Res. Lett. 38 (2011a) L10401, https:// doi.org/10.1029/2011GL047265
- [14] J.B. Randolph, M.O. Saar, Impact of reservoir permeability on the choice of subsurface geothermal heat exchange fluid: CO₂ versus water and native brine, Trans. Geoth. Resour. Counc. 35 (2011b) 521–526.
- [15] M.O. Saar, J.B. Randolph, T.H. Kuehn, Carbon dioxide-based geothermal energy generation systems and methods related thereto, & The Regents of the University of Minnesota, U.S. Patent No. 8 (316) (2012) 955. Canada Patent No. 2 753 393
- [16] A.D. Atrens, H. Gurgenci, V. Rudolph, CO₂ thermosiphon for competitive
- geothermal power generation, Energy Fuels 23 (2009) 553–557. [17] B.M. Adams, M.R. Fleming, J.M. Bielicki, J. Hansper, S. Glos, M. Langer, M. Wechsung, M.O. Saar, Grid Scale Energy Storage Using CO2 in Sedimentary Basins: the Cost of Power Flexibility, European Geothermal Congress, Hague, Netherlands, 2019, pp. 11-14. June.
- [18] T. Buscheck, J. Bielicki, T. Edmunds, T. Hao, Y. Sun, J. Randolph, M.O. Saar, Multi-fluid geo-energy systems: using geologic CO2 storage for geothermal energy production and grid-scale energy storage in sedimentary basins, Geosphere 12 (3) (2016) 1–19.
- [19] M.R. Fleming, B.M. Adams, J.B. Randolph, J.D. Ogland-Hand, T.H. Kuehn, T.A. Buscheck, J.M. Bielicki, M.O. Saar, High efficiency and large-scale subsurface energy storage with CO2, in: Proceedings, 43rd Workshop on Geothermal Reservoir Engineering, Stanford University, Stanford, CA, 2018. February 12-14, 2018.
- [20] M.R. Fleming, B.M. Adams, M.O. Saar, Using sequestered CO2 as geothermal working fluid to generate electricity and store energy, in: World Geothermal Congress, Reykjavik, 21 May to 26 May, 2021, 2021.
- [21] J. Ogland-Hand, J.M. Bielicki, Y. Wang, B.M. Adams, T.A. Buscheck, M.O. Saar, The value of bulk energy storage for reducing CO2 emissions and water requirements from regional electricity systems, Energy Convers. Manag. 181 (2019) 674-685, https://doi.org/10.1016/j.enconman.2018.12.019.
- [22] J. Ogland-Hand, J.M. Bielicki, B.M. Adams, E.S. Nelson, T.A. Buscheck, M.O. Saar, R. Sioshansi, The Value of CO₂-bulk Energy Storage with Wind in Transmission Constrained Electric Power Systems, Energy Convers. Manage. (2020), https:// doi.org/10.1016/j.enconman.2020.113548
- [23] Massachusetts Institute of Technology (MIT), The Future of Geothermal Energy: Impact of Enhanced Geothermal Systems (EGS) on the United States in the 21st Century, 2006. http://www.eere.energy.gov/geothermal/future_ geothermal.html.
- [24] F.V. Bekun, A.A. Alola, S.A. Sarkodie, Toward a sustainable environment: Nexus between CO2 emissions, resource rent, renewable and nonrenewable energy in 16-EU countries, Sci. Total Environ. 657 (2019) 1023-1029, https://doi.org/ 10.1016/j.scitotenv.2018.12.104.
- [25] Environmental Protection Agency (EPA), Inventory of U.S. Greenhouse Gas Emissions: Sinks and Sources, 2012. EPA 430-R-14-003, http://www.epa.gov/ climatechange/emissions/usinventoryreport.html.
- [26] Energy Information Agency (EIA), Electric power monthly. January, Available at: http://www.eia.gov/electricity/monthly/, 2015.
- [27] IRENA, Renewable Power Generation Costs in 2018, International Renewable Energy Agency, Abu Dhabi, 2019.
- [28] D. Brown, A hot dry rock geothermal energy concept utilizing supercritical CO2 instead of water, in: Proceedings of the Twenty-Fifth Workshop on Geothermal Reservoir Engineering, Stanford University, Stanford, California, 2000. January 24-26, 2000.
- [29] K. Pruess, Enhanced geothermal systems (EGS) using CO₂ as working fluid—a novel approach for generating renewable energy with simultaneous sequestration of carbon, Geothermics 35 (2006) 351-367.
- [30] F. Amann, V. Gischig, K. Evans, J. Doetsch, R. Jalali, B. Valley, H. Krietsch, N. Dutler, L. Villiger, B. Brixel, M. Klepikova, A. Kittilä, C. Madonna, S. Wiemer, M.O. Saar, S. Loew, T. Driesner, H. Maurer, D. Giardini, The seismo-hydromechanical behaviour during deep geothermal reservoir stimulations: open questions tackled in a decameter-scale in-situ stimulation experiment, Solid Earth (2018) 115-137, https://doi.org/10.5194/se-9-115-2018.

- [31] V.S. Gischig, D. Giardini, F. Amann, M. Hertrich, H. Krietsch, S. Loew, H. Maurer, L. Villiger, S. Wiemer, F. Bethmann, B. Brixel, J. Doetsch, N. Gholizadeh Doonechaly, T. Driesner, N. Dutler, K.F. Evans, M. Jalali, D. Jordan, A. Kittilä, X. Ma, P. Meier, M. Nejati, A. Obermann, K. Plenkers, M.O. Saar, A. Shakas, B. Valley, Hydraulic Stimulation and Fluid Circulation Experiments in Underground Laboratories: Stepping up the Scale towards Engineered Geothermal Systems, Geomechanics for Energy and the Environment, 2019, https://doi.org/10.1016/j.gete.2019.100175.
- [32] A. Kittilä, M.R. Jalali, M. Somogyvári, K.F. Evans, M.O. Saar, X.-Z. Kong, Characterization of the effects of hydraulic stimulation with tracer-based temporal moment analysis and tomographic inversion, Geothermics 86 (2020) 101820, https://doi.org/10.1016/j.geothermics.2020.101820.
- [33] A.D. Atrens, H. Gurgenci, V. Rudolph, Electricity generation using a carbondioxide thermosiphon, Geothermics 39 (2010) 161-169.
- K.F. Beckers, M.Z. Lukawski, B.J. Anderson, M.C. Moore, J.W. Tester, Levelized costs of electricity and direct-use heat from enhanced geothermal systems, J. Renew. Sustain. Energy 6 (2014), 013141, https://doi.org/10.1063/ 1.4865575.
- [35] K.F. Beckers, K. McCabe, GEOPHIRES v2.0; updated geothermal technoeconomic simulation tool, Geoth. Energy 7 (2019) 5, https://doi.org/ 10 1186/s40517-019-0119-6
- [36] M.G. Grimm Lima, P. Schädle, D. Vogler, M.O. Saar, X.Z. Kong, Impact of Effective Normal Stress on Capillary Pressure in a Single Natural Fracture, European Geothermal Congress, Den Haag, The Netherlands, 2019, pp. 11–14.
- M.G. Grimm Lima, P. Schädle, C.P. Green, D. Vogler, M.O. Saar, X.Z. Kong, Permeability impairment and salt precipitation patterns during CO₂ injection into single natural brine-filled fractures, Water Resour. Res. (2020), https:// doi org/10 1029/2020WR027213
- W.L. Ellsworth, D. Giardini, J. Townend, S. Ge, T. Shimamoto, Triggering of the Pohang, Korea, earthquake (Mw 5.5) by enhanced geothermal system stimulation, Seismol Res. Lett. 90 (5) (2019), https://doi.org/10.1785/0220190102.
- B.C. Gordalla, U. Ewers, F.H. Frimmel, Hydraulic fracturing: a toxicological threat for groundwater and drinking-water? Environ. Earth Sci. 70 (2013) 3875-3893
- [40] A. Kissinger, R. Helmig, A. Ebigbo, H. Class, T. Lange, M. Sauter, M. Heitfeld, J. Klünker, W. Jahnke, Hydraulic fracturing in unconventional gas reservoirs: risks in the geological system, part 2, Environ. Earth Sci. 70 (2013) 3855-3873
- [41] J.L. Coleman, S.M. Cahan, Preliminary Catalog of the Sedimentary Basins of the United States: U.S. Geological Survey Open-File Report 2012-1111, 2012. http://pubs.usgs.gov/of/2012/1111/.
- [42] National Energy Technology Laboratory (NETL), Carbon Storage Atlas, fifth ed., 2015 https://www.netl.doe.gov/coal/carbon-storage/strategic-programsupport/natcarb-atlas.
- [43] United States Geologic Survey (USGS), National Assessment of Geologic Carbon Dioxide Storage Resources-Data, 2013. Data series 774, version 1.1, http://pubs.usgs.gov/ds/774/.
- P.A. Allen, J.R. Allen, Basin Analysis: Principles and Application to Petroleum Play Assessment, John Wiley & Sons, 2013.
- G. Einsele, Sedimentary Basins: Evolution, Facies, and Sediment Budget, Springer Science & Business Media, 2000.
- J. Hartmann, N. Moosdorf, The new global lithological map database GLiM: a representation of rock properties at the Earth surface, G-cubed 13 (12) (2012), https://doi.org/10.1029/2012GC004370.
- [47] T.R. Elliot, T.A. Buscheck, M. Celia, Active CO2 reservoir management for sustainable geothermal energy extraction and reduced leakage, Greenhouse Gases: Sci. Technol. 3 (2013) 50-65.
- [48] N. Garapati, J.B. Randolph, J.L. Valencia, M.O. Saar, CO₂-Plume Geothermal (CPG) heat extraction in multi-layered geologic reservoirs, Energy Procedia 63 2014b) 7631-7643.
- [49] G.L. Mines, (2016). GETEM User Manual. Idaho National Laboratory, INL/EXT-16-38751. https://workingincaes.inl.gov/SiteAssets/CAES%20Files/FORGE/inl_ ext-16-38751%20GETEM%20User%20Manual%20Final.pdf.
- [50] N. Garapati, J.B. Randolph, M.O. Saar, Total heat energy output from, thermal energy contributions to, and reservoir development of CO₂ Plume Geothermal (CPG) systems, in: Proceedings, Thirty-Ninth Workshop, Geothermal Reservoir Engineering Stanford University, Stanford, California, 2014a. February 24-
- [51] N. Garapati, B.M. Adams, M.R. Fleming, T.H. Kuehn, M.O. Saar, Combining brine or CO2 geothermal preheating with low-temperature waste heat: a higher-efficiency hybrid geothermal power system, Journal of CO₂ Utilization 42 (2020) 101323, https://doi.org/10.1016/j.jcou.2020.101323
- B. Adams, On the Power Performance and Integration of Carbon-Dioxide Plume Geothermal (CPG) Electrical Energy Production, PhD Thesis. University of Minnesota, 2015. http://hdl.handle.net/11299/175183.
- K. Pruess, The TOUGH codes a family of simulation tools for multiphase flow and transport processes in permeable media, Vadose Zone J. 3 (2004)
- [54] S. Klein, Engineering Equation Solver, F-Chart Software, Madison, WI, 2017.
- J.M. Bielicki, B.M. Adams, H. Choi, B. Jamiyansuren, S.J. Taff, T.A. Buscheck, J.D. Ogland-Hand, J.B. Randolph M.O. Saar, (in review). Cost-competitive Geothermal Electricity for Geologic CO2 Storage, Energy Convers. Manag..
- K. Pruess, ECO2N: a TOUGH2 fluid property module for mixtures of water, NaCl, and CO₂, in: Rep. LBNL-57952, Lawrence Berkeley National Laboratory, Berkeley, 2005.

- [57] N. Spycher, K. Pruess, A model for thermophysical properties of CO₂-brine mixtures at elevated temperatures and pressures, in: Proceedings Thirty-Sixth Workshop on Geothermal Reservoir Engineering, Stanford University, Stanford, CA, 2011. January 31 — February 2, SGP-TR-191.
- [58] J. Ezekiel, B.M. Adams, M.O. Saar, & A. Ebigbo, (in review). Numerical analysis and optimization of the performance of CO₂-Plume Geothermal (CPG) production wells and implications for electric power generation. Geothermics.

 [59] R. Span, W. Wagner, A new equation of state for carbon dioxide covering the

- fluid region from the triple-point temperature to 1100 K at pressures up to 800 MPa, J. Phys. Chem. Ref. Data 25 (1996) 1509–1596.

 [60] H.J. Ramey Jr., Wellbore heat transmission, Soc. Petrol. Eng. 96 (1962) 427–435.
- [61] J.B. Randolph, B. Adams, T.H. Kuehn, M.O. Saar, Wellbore heat transfer in CO₂based geothermal systems, Trans. Geoth. Resour. Counc. 36 (2012) 549–554.
- [62] H.C.H. Armstead, J.W. Tester, Heat Mining, University Press, Cambridge, 1987.